Volume 52, issue 5, May 2010 ISSN 0010-938X

ELSEVIER

CORROSION SCIENCE

The Journal on Environmental Degradation of Materials and its Control

Editor-in-Chief: G. T. BURSTEIN, University of Cambridge, U.K.

An Official Journal of the Institute of Corrosion

CONTENTS

Contents continued on outside back matter

http://www.elsevier.com/locate/corsci

Corrosion Science 52 (2010) 1625–1634

Contents lists available at ScienceDirect

Corrosion Science

journal homepage: www.elsevier.com/locate/corsci

Solution chemistry of Mo(III) and Mo(IV): Thermodynamic foundation for modeling localized corrosion

Peiming Wang [a], Leslie L. Wilson [b], David J. Wesolowski [b], Jörgen Rosenqvist [b,1], Andrzej Anderko [a,*]

[a] OLI Systems Inc., 108 American Road, Morris Plains, NJ 07950, USA
[b] Chemical Sciences Division, Oak Ridge National Laboratory, 1 Bethel Valley Road, Oak Ridge, TN 37831-6110, USA

ARTICLE INFO

Article history:
Received 13 August 2009
Accepted 18 January 2010
Available online 22 January 2010

Keywords:
B. Modeling studies
B. Electrochemical calculation
C. Thermodynamic diagrams

ABSTRACT

To investigate the behavior of molybdenum dissolution products in systems that approximate localized corrosion environments, solubility of Mo(III) in equilibrium with solid MoO_2 has been determined at 80 °C as a function of solution acidity, chloride concentration and partial pressure of hydrogen. The measurements indicate a strong increase in solubility with acidity and chloride concentration and a weak effect of hydrogen partial pressure. The obtained results have been combined with literature data for systems containing Mo(III), Mo(IV), and Mo(VI) in solutions to develop a comprehensive thermodynamic model of aqueous molybdenum chemistry. The model is based on a previously developed framework for simulating the properties of electrolyte systems ranging from infinite dilution to solid saturation or fused salt limit. To reproduce the measurements, the model assumes the presence of a chloride complex of Mo(III) (i.e., $MoCl^{2+}$) and hydrolyzed species ($MoOH^{2+}$, $Mo(OH)_2^{+}$, and $Mo(OH)_3^{0}$) in addition to the Mo^{3+} ion. The model generally reproduces the experimental data within experimental scattering and provides a tool for predicting the phase behavior and speciation in complex, concentrated aqueous solutions. Thus, it provides a foundation for simulating the behavior of molybdenum species in localized corrosion environments.

1. Introduction

Molybdenum is a key component of numerous corrosion-resistant alloys. Various studies have been focused on understanding the effect of molybdenum on the initiation and stabilization of localized corrosion [1–5]. However, much less attention has been devoted to the solution chemistry of molybdenum in localized corrosion environments. It is well known that environments within corroding crevices or pits are acidic, reducing, and contain high concentrations of chlorides and/or other aggressive ions. Dissolution of an alloy within a localized corrosion environment leads to the formation of lower oxidation states of Mo, which may be, at a later stage, oxidized to the 6+ oxidation state. Thus, the thermodynamic behavior of lower oxidation states of Mo is important for understanding the stabilization and propagation of localized corrosion of Mo-containing alloys. In particular, solubility behavior and speciation are of great interest because they determine the composition envelope and pH of alloy dissolution products. The key oxidation state appears to be 3+ because it is associated with a high solubility of Mo(III) species [6,7].

Relatively abundant experimental data are available for Mo in the 6+ oxidation state, which makes it possible to determine the thermodynamic properties of Mo(VI) species and their solutions with reasonable accuracy. There is a very limited amount of thermodynamic data for the Mo(III) and Mo(IV) oxidation states. In particular, there is no published information on the properties of Mo(III) ions in aqueous chloride solutions and on the phase equilibrium boundary between Mo(III) and Mo(IV) species (the latter being in the form of solid MoO_2). This boundary is of particular importance for quantifying the behavior of Mo in localized corrosion environments because it delimits the range of conditions under which molybdenum remains completely dissolved in solution in the form of Mo(III) ions. At pH and/or potential values above the Mo(III)/Mo(IV) boundary, Mo(III) species convert to solid MoO_2, thus imposing a step change in the behavior of corrosion products. The objective of this study is to provide the necessary information on the phase behavior of Mo(III) and Mo(IV) to fill this important gap in our understanding of Mo chemistry.

In this study, we first report new experimental measurements of solubilities of Mo(III) species in equilibrium with MoO_2 as a function of acidity, chloride concentration and hydrogen partial pressure. Then, we use the new data in conjunction with the

* Corresponding author. Fax: +1 973 539 5922.
E-mail address: aanderko@olisystems.com (A. Anderko).
[1] Present address: School of Earth and Environment, University of Leeds, Leeds LS2 9LT, United Kingdom.

0010-938X/$ - see front matter © 2010 Elsevier Ltd. All rights reserved.
doi:10.1016/j.corsci.2010.01.032

available literature information for Mo(VI) and Mo(VI)/Mo(IV) aqueous systems to develop a comprehensive thermodynamic model for molybdenum species in aqueous chloride environments. This model is established using a previously developed thermodynamic framework for electrolyte systems [8–10], which is particularly suitable for complex, concentrated solutions. It is expected that this model will provide a useful tool for simulating the chemistry of localized corrosion environments.

2. Experimental

All experimental solutions were prepared from reagent grade chemicals and distilled de-ionized water (18.3 MΩ cm resistivity). The molybdenum dioxide solid was obtained from Alfa Aesar (99% metal basis, Lot # E21S044). X-ray diffraction patterns collected on a Siemens D5005 diffractometer using Cu Kα radiation showed distinct peaks for MoO_2, with minor contributions from the hydrated form $MoO_3{\cdot}0.34H_2O$. The hydrated phase was estimated to be less than 3% of the total.

The dissolution experiments were performed in a reaction vessel consisting of a Teflon cup and cover plug (which fits loosely to allow gas equilibration within the pressure vessel, but prevents debris and condensates from dropping into the experimental solution), placed inside a Hastelloy B pressure vessel. The pressure vessel head contains a stainless steel capillary connection to the gas inlet/outlet and pressure-monitoring manifold, and a platinum tube is also sealed into the head but extends through the head and the Teflon plug to near the bottom of the Teflon cup and has a submicron Pt/Au filter affixed to the submerged end that allows primary filtering of the suspended solid during sampling of the experimental solution. The suspension only comes into contact with Teflon and precious metals. The suspension is kept homogeneous by a Teflon-coated stir bar. The platinum sample tube is connected to a titanium sampling valve kept near room temperature outside the furnace. The general features of the reaction system are described by Palmer et al. [11]. We did not continuously monitor the solution pH during these experiments, since past experience indicated that reduced molybdenum species affect the response of the platinum/H_2 electrodes used in the experiments described by Palmer et al. [11].

Each experiment was started by weighing the appropriate amounts of MoO_2(s) (1–2 g) and solution (~50 g) into the Teflon cup, along with the Teflon-coated stirring bar. The pressure vessel was sealed as fast as possible and the head space was flushed with hydrogen gas five times before the experimental gas atmosphere (either pure hydrogen or a mixture of hydrogen and argon) was introduced. All gases were ultra high purity (99.999%) grade. The specific pressures and gas mixtures for each experiment are listed in Table 1. The vessel was then placed in an aluminum block within a Marshall-type tube furnace that had been preheated to 80 °C, and the system was allowed to thermally equilibrate. The temperature of the furnace is controlled to within ±0.1 °C and the internal pressure is monitored (±1 bar) with strain-gauge transducers.

Sampling was conducted after equilibration at the desired P–T conditions for at least 20 h. An aliquot of sample solution (~1–2 g) was collected and discarded before each experimental sample was collected. Experimental samples were extracted at temperature through the *in situ* submicron filter and platinum sampling tube, as well as a 0.2 micron PVDF syringe filter attached to the high pressure titanium valve. A pre-weighted polyethylene/polypropylene syringe, partially filled with a known mass of ultra high purity acid (either 0.2% HNO_3 or 4% HCl), was attached to the syringe filter and the sample was allowed to slowly diffuse into the acid. After sampling, the syringe was again weighed, excess gas was expelled, and the syringe capped to prevent reaction with the lab atmosphere.

The total concentration of soluble Mo in each sample was determined by atomic absorption spectrophotometry using a Varian AA240Z spectrometer equipped with a GTA120 graphite tube atomizer, following Varian's standard protocol for Mo analyses. The practical detection limit was $\sim 5\bullet 10^{-8}$ molal (m). Measured total concentrations are reported in Table 1. The partial pressure of hydrogen in each experiment was calculated from the measured total pressure and temperature (Table 1), assuming ideal gas behavior of the $H_2 + H_2O \pm Ar$ gas phase, and the vapor pressure of water in NaCl solutions with salinities equal to the experimental solutions, using the model of Archer [12]. Since the solubility of MoO_2 in these experiments is only weakly dependent on the H_2 partial pressure, this approach, with an estimated uncertainty of ~10% in the tabulated partial pressure, is sufficiently accurate.

3. Thermodynamic model

To analyze the experimental data and to determine the necessary thermodynamic parameters, we use a thermodynamic frame-

Table 1
Results of measurements of solid–liquid equilibria in Mo(III)–Mo(IV)–H–Na–Cl systems.

Sample ID	T(°C)	P, total (bar)	$P(H_2)$ (bar)	Starting solution composition (molal)			Total dissolved Mo (molal)
				H^+	Na^+	Cl^-	
MolyIVa-001	80.71	65.5	65	0.0992	0	0.0992	0.0001291
MolyIVa-002	80.74	67.5	67	0.0992	0	0.0992	0.0001368
MolyIVb-001	80.68	72.6	3.6	0.1008	0	0.1008	0.0003890
MolyIVb-002	80.70	70.1	3.5	0.1008	0	0.1008	0.0003396
MolyIVc-001[a]	80.66	17.1	1.5	0.0996	0.9003	0.9999	0.009954
MolyIVd-001	80.80	10.1	1	0.1001	0.9	1.0001	0.005929
MolyIVe-001	80.80	27.7	3.9	0.1001	4.9001	5.0002	0.01507
MolyIVe-002	80.70	46.1	23.2	0.1001	4.9001	5.0002	0.01042
MolyIVe-003	80.67	71.2	35.9	0.1001	4.9001	5.0002	0.009397
MolyIVf-001	80.74	26.3	3.7	0.0999	0.8998	0.9997	0.001660
MolyIVf-002	80.74	44.7	20.5	0.0999	0.8998	0.9997	0.0004355
MolyIVf-003	80.78	71.7	49.3	0.0999	0.8998	0.9997	0.0003459
MolyIVg-001	80.79	27	3.8	0.9999	4.0	4.9999	0.02388
MolyIVg-002	80.68	26	3.6	0.9999	4.0	4.9999	0.02312
MolyIVg-003	80.71	44.5	22.1	0.9999	4.0	4.9999	0.02291
MolyIVg-004	80.75	43.2	21.4	0.9999	4.0	4.9999	0.02178
MolyIVh-001	80.87	25.9	3.6	5.0	0	5.0	0.03381
MolyIVh-002	80.82	44.3	23.5	5.0	0	5.0	0.03908
MolyIVh-003	80.83	62.2	43	5.0	0	5.0	0.03733

[a] Loss of pressure observed.

work that has been previously developed by Wang et al. [8–10] for mixed-solvent electrolyte systems. This framework is capable of reproducing the properties of multicomponent solutions that contain both ions and neutral molecules or ion pairs. It is applicable to systems ranging from infinite dilution to the fused salt limit and, therefore, it is suitable for the concentration ranges investigated here. The model was described in detail in previous papers [8–10] and, therefore, only a brief summary is given here to introduce the parameters that need to be determined.

The thermodynamic framework combines a comprehensive treatment of chemical equilibria with separate models for the excess Gibbs energy of the mixture and standard-state properties of individual species. The excess Gibbs energy model represents the solution nonideality whereas the standard-state property model represents the behavior of species at infinite dilution. The excess Gibbs energy is expressed as

$$\frac{G^{ex}}{RT} = \frac{G^{ex}_{LR}}{RT} + \frac{G^{ex}_{II}}{RT} + \frac{G^{ex}_{SR}}{RT} \tag{1}$$

where G^{ex}_{LR} represents the contribution of long-range electrostatic interactions, G^{ex}_{II} accounts for specific ionic (ion–ion and ion–molecule) interactions and G^{ex}_{SR} is a short-range contribution resulting from intermolecular interactions. The activities, $a_i(T,\boldsymbol{x})$, and activity coefficients, $\gamma_i(T,\boldsymbol{x})$, of individual species can be obtained from the excess Gibbs energy by differentiation with respect to the number of moles [13].

The long-range interaction contribution is calculated from the Pitzer–Debye–Hückel formula [14] expressed in terms of mole fractions and symmetrically normalized, *i.e.*,

$$\frac{G^{ex}_{LR}}{RT} = -\left(\sum_i n_i\right)\frac{4A_x I_x}{\rho}\ln\left(\frac{1+\rho I_x^{1/2}}{\sum_i x_i[1+\rho(I^0_{x,i})^{1/2}]}\right) \tag{2}$$

where the sum is over all species, I_x is the mole fraction-based ionic strength, $I^0_{x,i}$ represents the ionic strength when the system composition reduces to a pure component i, *i.e.*, $I^0_{x,i} = 0.5z_i^2$; ρ is related to the hard-core collision diameter (ρ = 14.0 and A_x is given by

$$A_x = \frac{1}{3}(2\pi N_A d_s)^{1/2}\left(\frac{e^2}{4\pi\varepsilon_0\varepsilon_s k_B T}\right)^{3/2} \tag{3}$$

where d_s and ε_s are the molar density and relative permittivity of the solvent, respectively. The specific ion-interaction contribution is calculated from an ionic strength-dependent, symmetrical second virial coefficient-type expression [8]:

$$\frac{G^{ex}_{II}}{RT} = -\left(\sum_i n_i\right)\sum_i\sum_j x_i x_j B_{ij}(I_x) \tag{4}$$

where $B_{ij}(I_x) = B_{ji}(I_x), B_{ii} = B_{jj} = 0$ and the ionic strength dependence of B_{ij} is given by

$$B_{ij}(I_x) = b_{ij} + c_{ij}\exp(-\sqrt{I_x + a_1}) \tag{5}$$

and where b_{ij} and c_{ij} are binary interaction parameters between species i and j and a_1 is set equal to 0.01. Within the temperature range that is of interest here, the parameters b_{ij} and c_{ij} are calculated as

$$b_{ij} = b_{0,ij} + b_{1,ij}T + b_{2,ij}/T \tag{6}$$

$$c_{ij} = c_{0,ij} + c_{1,ij}T + c_{2,ij}/T \tag{7}$$

For interactions between many cation–anion pairs, it is sufficient to use temperature-independent parameters b_{ij} and c_{ij}. In such cases, only the first coefficient on the right-hand side of Eqs. (6) and (7) is used. Finally, the short-range interaction contribution in Eq. (1) is calculated from the UNIQUAC equation [15]. This term is used for interactions between neutral molecules or between ions and neutral molecules. However, for the molybdenum systems considered here, the short-range term is unnecessary and all interactions are accounted for by Eq. (4).

The standard-state chemical potentials for aqueous species, $\mu^o_i(T,P)$, are calculated as functions of temperature and pressure using the Helgeson–Kirkham–Flowers–Tanger (HKF) equation of state [16,17]. The parameters of the HKF model have been published for a large number of aqueous species including ions and ion pairs [18–21]. A methodology for combining the standard-state properties calculated from the HKF model with the activity coefficients calculated from the excess Gibbs energy model (Eq. 1) has been described by Wang et al. [8].

Both the standard-state properties and the excess Gibbs energy model are necessary to compute chemical equilibria in the solution. Each chemical reaction can be written as

$$\sum \nu_i M_i = 0 \tag{8}$$

and its equilibrium state is defined by

$$\sum \nu_i \mu_i = 0 \tag{9}$$

where μ_i is the chemical potential of species i. Eq. (7) represents both homogeneous reactions (between solution species) and heterogeneous (dissolution/precipitation) reactions. The chemical potential of each ionic or neutral species i is determined by its standard-state contribution, $\mu^o_i(T,P)$, and its activity, $a_i(T,\boldsymbol{x})$, which is in turn calculated using the activity coefficient, $\gamma_i(T,\boldsymbol{x})$, *i.e.*,

$$\mu_i(T,P,x) = \mu^0_i(T,P) + RT\ln x_i\gamma_i(T,\mathbf{x}) \tag{10}$$

where $\mu^0_i(T,P)$ is calculated as a function of temperature and pressure from the HKF equation of state, $\gamma_i(T,\mathbf{x})$ is obtained as a function of temperature and the composition vector $\mathbf{x}$ by standard thermodynamic differentiation of the excess Gibbs energy (Eqs. (1–7) and the product $x_i\gamma_i(T,\mathbf{x})$ constitutes the activity, $a_i(T,\boldsymbol{x})$, of species i. While the activity coefficients of individual ionic species $\gamma_i(T,\mathbf{x})$ are not accessible experimentally, they can be calculated after the excess Gibbs energy (Eqs. (1–7) is parameterized based on empirical data. In this way, the $\gamma_i(T,\mathbf{x})$ coefficients are made consistent, within the combined accuracy of the data and the model, with the mean activity coefficients of solutes, which are measurable and are a reflection of properties such as solubilities, vapor–liquid equilibria, electromotive force, etc.

Calculation of solid solubilities and speciation equilibria in the solution requires solving a system of multiple equations as defined by Eqs. (9–10) for each individual homogeneous and precipitation reaction. Procedures for solving chemical and phase equilibria in electrolyte systems have been described by Zemaitis et al. [13] and Rafal et al. [22].

4. Determination of parameters

Molybdenum species are known to exist in a large number of oxidation states ranging from 0 to 6+ [6]. However, due to the limited availability of thermodynamic data, it is possible to characterize the properties of only the most important oxidation states, i.e., Mo(III), Mo(IV), and Mo(VI). A substantial amount of experimental data exists in the literature for Mo(VI) species both in the absence and presence of chloride ions. Further, there is a limited amount of information on the behavior of Mo(IV), which exists in the form of the solid MoO_2 phase. This literature information has been used here in conjunction with the new solubility results obtained under reducing conditions. The model parameters have been regressed jointly for (1) Mo(III) speciation, (2) Mo(III)/Mo(IV) phase boundary, (3) Mo(IV)/Mo(VI) phase boundary and (4) phase equilibria in Mo(VI) systems.

For Mo(III) speciation, the hydrolysis data of Mit'kina et al. [23] have been analyzed. These data indicate the presence of three

hydrolyzed Mo(III) species, i.e., $Mo(OH)^{2+}$, $Mo(OH)_2^{+}$, and $Mo(OH)_{3(aq)}$ and provide the equilibrium constants for their formation. These constants allow us to constrain the Gibbs energies of formation of $Mo(OH)^{2+}$, $Mo(OH)_2^{+}$, and $Mo(OH)_{3(aq)}$ relative to the Gibbs energy of formation of the Mo^{3+} ion. However, the equilibrium concentrations of various Mo(III) species calculated on the basis of these thermochemical data indicate that the $Mo(OH)_{3(aq)}$ species is overwhelmingly stable in presence of reducing/oxidizing agents, which would result in unreasonable E-pH diagrams. In addition, these data are inconsistent with the solubilities of MoO_2 measured by Kudrin [25] at elevated temperatures and pressures under oxidizing conditions where the primary oxidation state of molybdenum in MoO_2-saturated solutions was confirmed to be Mo(VI). The thermochemical properties of the hydrolyzed forms were therefore adjusted so that the MoO_2 solubility under both oxidizing (at the Mo(IV)/Mo(VI) boundary) and reducing (at the Mo(III)/Mo(IV) boundary) conditions can be reasonably reproduced.

For the Mo(III)/Mo(IV) boundary, the data reported in Table 1 have been used. Since these data provide equilibrium solubilities of MoO_2 in Mo(III) solutions, they allow us to constrain the Gibbs energy of formation of Mo^{3+} relative to that of MoO_2. Further, since they were obtained in relatively concentrated chloride solutions, they allow us to postulate the presence of chloride complexes of Mo^{3+} and to calculate interaction parameters between the solution species that are present in high concentrations. The predominance of Mo(III) species in the sample solutions was confirmed using UV spectroscopy. For this purpose, we utilized the results of Kekesi et al. [24], who recorded spectra for Mo solutions both before and after reducing Mo using Zn powder and found that Mo(III) has characteristic peaks around 370 and 480 nm, while Mo in higher oxidation states shows peaks at considerably higher wavelengths (e.g. ~710 nm). The spectra for two of our sample solutions (Table 1) are presented in Fig. 1, clearly showing the peaks attributed to Mo(III). Also, the absence of peaks at higher wavelengths indicates that Mo in higher oxidation states is either completely absent or present at negligible concentrations only. The observed difference between the two spectra shown in Fig. 1 can be attributed to the slightly different Mo concentrations in the two experiments due to differences in the reducing atmosphere (i.e. P_{H_2} and P_{total}).

For the Mo(IV)/Mo(VI) boundary, we have utilized the data of Kudrin [25], which provide the conditions for the oxidative dissolution of MoO_2 as a function of oxygen fugacity. These data provide a constraint for the Gibbs energy of formation of MoO_2 relative to that of MoO_4^{2-}.

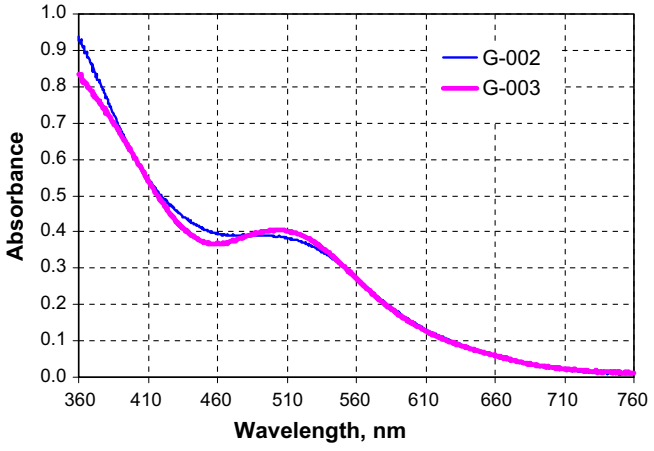

Fig. 1. UV spectra of MoO_2-saturated solutions (Mo ~ 0.023 m) in 1.0 m HCl and 4.0 m NaCl at P_{H_2} =3.6 bar, P_{total} =26 bar (G-002) and P_{H_2} =22.1 bar, P_{total} =44.5 bar (G-003).

Finally, for Mo(VI) equilibria, solubility data have been used for MoO_3 in water [26–30] and in HCl solutions [28,30,31]. The solubilities in water make it possible to determine the Gibbs energies of formation of the MoO_3 hydrates that are stable in aqueous solutions. The solubilities in HCl allow us to constrain the properties of chloride complexes and interaction parameters. The presence of chloride oxy complexes of Mo(VI) is likely in view of the available structural data [6] and, therefore, such complexes need to be considered in parameter regression.

In practice, Mo(VI) phase equilibria have been analyzed first because the thermochemical properties of the base ions MoO_4^{2-} and $HMoO_4^{-}$ are known with a good accuracy [18,19] and did not need to be modified. Further, the polynuclear species $Mo_7O_{24}^{6-}$ and $HMo_7O_{24}^{5-}$ have been introduced on the basis of the equilibrium constants reported by Smith and Martell [32]. Although potentially multiple polynuclear Mo(VI) species may exist [6], thermodynamic data are insufficient to introduce a wider spectrum of polynuclear species. Furthermore, the species with seven Mo atoms appear to be more stable. Based on the thermochemical properties of these aqueous species, the standard Gibbs energy of formation and entropy of two stable solid Mo(VI) species, $MoO_3{\cdot}H_2O$ and $MoO_3{\cdot}2H_2O$ have been regressed. Then, solubilities of $MoO_3{\cdot}H_2O$ and $MoO_3{\cdot}2H_2O$ in hydrochloric acid were used to evaluate the thermochemical properties of a chloride-containing complex $H_4Mo_7O_{24}Cl^{3-}$ and its interaction parameters with H_3O^{+}. Such interaction parameters are necessary because the concentration of dissolved $H_4Mo_7O_{24}Cl^{3-}$ is substantial in concentrated HCl solutions. After determining the parameters of Mo(VI) species, the Gibbs energy of formation and entropy of MoO_2 have been evaluated on the basis of the data for the oxidative dissolution of MoO_2 [25]. With the properties of MoO_2 adjusted in this way, the Mo(III) solubility data (Table 1) have been regressed. This made it possible to adjust the thermochemical properties of the Mo^{3+} ions and to introduce the chloride complex $MoCl^{2+}$. The presence of this complex is very likely in view of the strong increase of solubility with chloride concentration. Although the presence of mixed-ligand species such as $Mo(OH)Cl^{+}$ is possible, their presence could not be determined from the available measurements and they were not needed to reproduce the data. The properties of the Mo^{3+} and $MoCl^{2+}$ ions have been regressed while simultaneously introducing their hydrolyzed forms $Mo(OH)^{2+}$, $Mo(OH)_2^{+}$, and $Mo(OH)_{3(aq)}$, with adjusted equilibrium constants of formation that yield reasonable speciation for the MoO_2/Mo(VI) equilibrium data of Kudrin [25]. In view of the high concentrations of protons and sodium ions in the systems reported in Table 1, interaction parameters between the H_3O^{+}, Na^{+}, Mo^{3+}, $Mo(OH)^{2+}$ and $MoCl^{2+}$ species have also been introduced. However, for simplicity, these parameters have been assigned a common, temperature-independent value.

In summary, the following parameters have been evaluated:

(i) The standard partial molar Gibbs energies of formation, $\Delta\overline{G}_f^0$, and entropies, $\overline{S}^0$, for the following Mo(III) aqueous species: Mo^{3+}, $Mo(OH)^{2+}$, $Mo(OH)_2^{+}$, $Mo(OH)_{3(aq)}$, and $MoCl^{2+}$ and the following Mo(VI) aqueous species: $Mo_7O_{24}^{6-}$, $HMo_7O_{24}^{5-}$, $H_2Mo_7O_{24}^{4-}$, $H_3Mo_7O_{24}^{3-}$, and $H_4Mo_7O_{24}Cl^{3-}$. In the case of Mo^{3+} and $MoCl^{2+}$, the parameters of the HKF equation [18–21] (i.e. $a_{HKF,1,\cdots 4}\, c_{HKF,1}, c_{HKF,2}\, \omega$ have been estimated from generalized correlations [21]. For the remaining Mo species, the HKF parameters have been set equal to zero. The Gibbs energies of formation, entropies, and HKF parameters are used to calculate the standard-state chemical potentials, $\mu_i^0(T,P)$, of individual species as described elsewhere [18–21].

(ii) The temperature-dependent ion-ion interaction parameters (Eqs. 6–7) between $H_4Mo_7O_{24}Cl^{3-}$ and H_3O^+, which reflect solution nonideality in Mo(VI)-chloride systems and make it possible to reproduce the solubility of MoO_3 in HCl solutions.
(iii) The temperature-independent ion-ion interaction parameters (Eqs. 6–7) between the dominant Mo(III) species, i.e., Mo^{3+}, $Mo(OH)^{2+}$, and $MoCl^{2+}$ and the remaining key species in the Mo(III) solutions investigated here, i.e., Cl^-, H_3O^+, Na^+, and $H_{2(aq)}$. For simplicity, it has been assumed that the interaction parameters involving the Mo^{3+}, $Mo(OH)^{2+}$, and $MoCl^{2+}$ species are the same. These parameters determine the activity coefficients of Mo species.
(iv) The Gibbs energy of formation, $\Delta_f G^o$, and entropy, S^o, of the three solid phases that may precipitate in the systems investigated here (i.e., MoO_3 H_2O, MoO_3 $2H_2O$, and MoO_2). These parameters determine the the standard-state chemical potentials of the solids $\mu_i^0(T,P)$ (c.f., Eq. 10) according to standard thermodynamics.

While evaluating the above parameters, the following parameters have been adopted from the literature and kept unchanged:

(i) The standard partial molar Gibbs energies of formation, entropies, and HKF parameters of the Cl^-, Na^+, H_3O^+, MoO_4^{2-}, and $HMoO_4^-$ ions, which are known from the literature [18–21].
(ii) The interaction parameters between base ions, especially Na^+ and Cl^-, which have been taken from previous studies [37].
(iii) The heat capacities of the solid phases, which have been taken from experimental data or estimated.

The model parameters are summarized in Tables 2–4. These tables also indicate the source of the parameters for individual species. Table 2 shows the standard-state properties and parameters of the HKF equation of state [16,17] for all Mo(III) and Mo(VI) ions that were taken into account in the model. Also, the parameters for the remaining solution ions (i.e., Cl^-, Na^+, and H_3O^+) are included for completeness. Table 2 also includes information about the sources of parameters for each species. Table 3 shows the binary parameters that are used in the ionic interaction term (Eqs. (6–7) to calculate activity coefficients. It should be noted that the complete temperature-dependent function for the interaction parameters (Eqs. 6–7) was needed only for the $H_4Mo_7O_{24}Cl^{3-}$–H_3O^+

Table 2
Parameters for individual ionic and neutral species: standard partial molar Gibbs energy of formation $\Delta\overline{G}_f^0$, entropy $\overline{S}^0$, and parameters of the Helgeson–Kirkham–Flowers equation of state [18–21] for standard partial molar thermodynamic properties ($a_{HKF,1,\cdots 4}, c_{HKF,1}, c_{HKF,2}, \omega$).

Species	$\Delta\overline{G}_f^0$ kJ mol^{-1}	$\overline{S}^0$ J mol^{-1}K^{-1}	$a_{HKF,1}$	$a_{HKF,2}$	$a_{HKF,2}$	$a_{HKF,3}$	$c_{HKF,1}$	$c_{HKF,2}$	ω
Cl^-[a]	−131.290	56.735	0.4032	480.1	5.563	−28470	−4.4	−57140	145600
Na^+[a]	−261.881	58.4086	0.1839	−228.5	3.256	−27260	18.18	−29810	33060
H_3O^+[a]	−237.175	69.99372	0.451232	−21.2711	−8.64735	20487.1	14.6773	16975.9	−13672.5
Mo^{3+}[b]	−45.834	−292.499[d]	−0.26567	−1426.8	11.3581	−21891	18.1083	−74992.	269044
$Mo(OH)^{2+}$[b]	−260.189	71.128							
$Mo(OH)_2^+$[b]	−471.687	117.152							
$Mo(OH)_{3(aq)}$[b]	−678.624	133.888							
$MoCl^{2+}$[b]	−165.078	−209.2	−0.060955	−926.98	9.3934	−23958.	83.84	180450.	184820
MoO_4^{2-}[a]	−838.474	37.3576	0.69651	270.95	18.6617	−28909	6.6829	−127102.	307770
$HMoO_4^-$[a]	−863.578	135.98	0.7732	1109.66	1.3908	−32376.	33.393	27912.	113590
$Mo_7O_{24}^{6-}$[c]	−5250.92	301.248							
$HMo_7O_{24}^{5-}$[c]	−5280.03	422.584							
$H_2Mo_7O_{24}^{4-}$[b]	−5322.93	493.712							
$H_3Mo_7O_{24}^{3-}$[b]	−5357.91	159.965							
$H_4Mo_7O_{24}Cl^{3-}$[b]	−5519.38	38.4794							

[a] All parameters were obtained from Shock et al. [18], Shock and Helgeson [19], and Shock et al. [20].
[b] Standard-state properties of the ion pairs were adjusted in this study based on multiproperty regressions; the estimated uncertainties of the Gibbs energy of formation and entropy are ±3 kJ mol^{-1} and ±10 J mol^{-1} K^{-1}, respectively. The HKF parameters ($a_{HKF,1,\cdots 4}, c_{HKF,1}, c_{HKF,2}, \omega$) were obtained from generalized correlations [21] for the Mo^{3+} and $MoCl^{2+}$ ions.
[c] Standard-state properties of these species were determined based on equilibrium constants from Smith and Martell [32].
[d] Calculated from the correlation of Sassani and Shock [36] rather than regressed.

Table 3
Binary parameters[a] used in the ionic interaction term to calculate the excess Gibbs energy (Eqs. 6–7 with temperature expressed in K).

Species i	Species j	$b_{0,ij}$	$b_{1,}ij$ (K^{-1})	$b_{2,ij}$ (K)	$c_{0,ij}$	$c_{1,ij}$ (K^{-1})	$c_{2,ij}$ (K)
$H_4Mo_7O_{24}Cl^{3-}$	H_3O^+	−1658.339	2.046453	301272.2	2542.723	−2.922353	−465363.2
Cl^-	Mo^{3+}	−2376.025	0	0	−698.6628	0	0
Cl^-	$Mo(OH)^{2+}$	−2376.025	0	0	−698.6628	0	0
Cl^-	$MoCl^{2+}$	−2376.025	0	0	−698.6628	0	0
H_3O^+	Mo^{3+}	2918.271	0	0	0	0	0
H_3O^+	$Mo(OH)^{2+}$	2918.271	0	0	0	0	0
H_3O^+	$MoCl^{2+}$	2918.271	0	0	0	0	0
Na^+	Mo^{3+}	2918.271	0	0	0	0	0
Na^+	$Mo(OH)^{2+}$	2918.271	0	0	0	0	0
Na^+	$MoCl^{2+}$	2918.271	0	0	0	0	0
$H_{2(aq)}$	Mo^{3+}	−2259.955	0	0	0	0	0
$H_{2(aq)}$	$Mo(OH)^{2+}$	−2259.955	0	0	0	0	0
$H_{2(aq)}$	$MoCl^{2+}$	−2259.955	0	0	0	0	0

[a] The estimated uncertainty of the binary parameters is ±5%.

Table 4
Thermodynamic parameters for solid phases: Gibbs energy of formation ($\Delta_f G^o$), entropy (S^o) and heat capacity coefficients (A, B, C, and D with temperature expressed in K).

Solid phase	$\Delta_f G^o$ (kJ mol^{-1})	S^o (J mol^{-1} K^{-1})	Cp (J mol^{-1} K^{-1}) = A + B/T + C/T^2 + DT^2			
			A	B	C	D
$MoO_3{\cdot}H_2O$	−908.748[a]	70.743[=a]	117.152[d]	0	0	0
$MoO_3{\cdot}2H_2O$	−1146.40[a]	89.082[a]	163.176[d]	0	0	0
MoO_2	−514.632[a]	8.029[a]	55.982[c]	0	0	0
Mo	0	28.57[b]	27.462[b]	−0.002406[b]	−2.770 10^{5}[b]	3.416 10^{-6}[b]

[a] Regressed using solubility data as described in the text; the estimated uncertainties of the Gibbs energy of formation and entropy are ±3 kJ mol^{-1} and ±10 J mol^{-1} K^{-1}, respectively.
[b] From Gurvich et al. [34].
[c] From NIST Webbook [35].
[d] Estimated using the NIST Webbook [35] value for MoO_3 and an increment for hydration water; the estimated uncertainty is ±10 J mol^{-1} K^{-1}.

interactions because they reflect the high concentrations of Mo(VI) in concentrated HCl solutions over a relatively wide temperature range. All remaining interaction coefficients are temperature-independent. Finally, Table 4 summarizes the properties of all four solid phases that are included in the model (i.e., $MoO_3{\cdot}H_2O$, $MoO_3{\cdot}2H_2O$, MoO_2, and Mo). The zero-valent Mo was not needed for the analysis of the solubility data but is included for completeness because it is necessary for the generation of E-pH diagrams. The Gibbs energies of formation and entropies of $MoO_3{\cdot}H_2O$, $MoO_3{\cdot}2H_2O$, and MoO_2 at reference conditions have been regressed from solubility data as described above whereas their heat capacities have been taken from literature sources or estimated based on data for anhydrous oxides. The data for Mo^0 have been taken entirely from literature sources as indicated in Table 4. These properties have been used to calculate the chemical potential of the solids as a function of temperature according to standard thermodynamics.

5. Results and discussion

The experimental and calculated concentrations of Mo(III) species in equilibrium with MoO_2 are shown in Fig. 2 as a function of partial pressure of hydrogen. Although hydrogen is necessary to stabilize Mo(III) in the solution, the dependence of solubility on H_2 partial pressure is rather weak. On the other hand, there is a strong dependence of Mo solubility on chloride concentration. This becomes evident by comparing the three lines that correspond to 5 m Cl^- solutions (i.e., the upper three lines in Fig. 2) with those for 0.1 m Cl^- (the lowest line) and 1 m Cl^- solutions (the dashed line). The strong effect of chloride is consistent with the formation of a $MoCl^{2+}$ complex at high Cl^- concentrations. The effect of acidity is also evident, but somewhat less pronounced than the effect of chlorides. The effect of acidity can be examined by comparing the three upper lines, which reflect the same chloride concentration

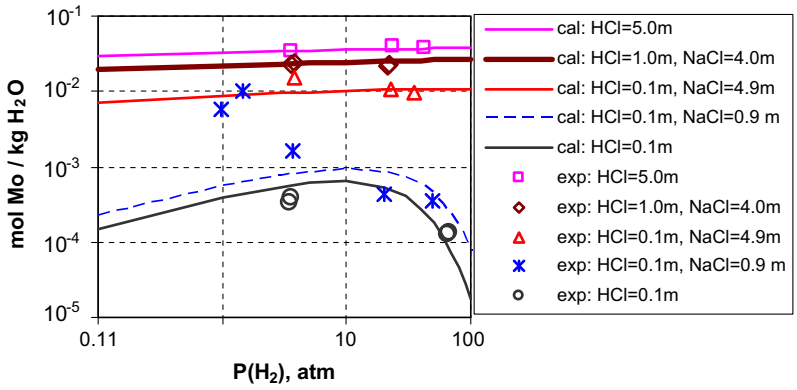

Fig. 2. Experimental and calculated concentration of Mo(III) in saturated solutions as a function of hydrogen partial pressure for various combinations of HCl and NaCl.

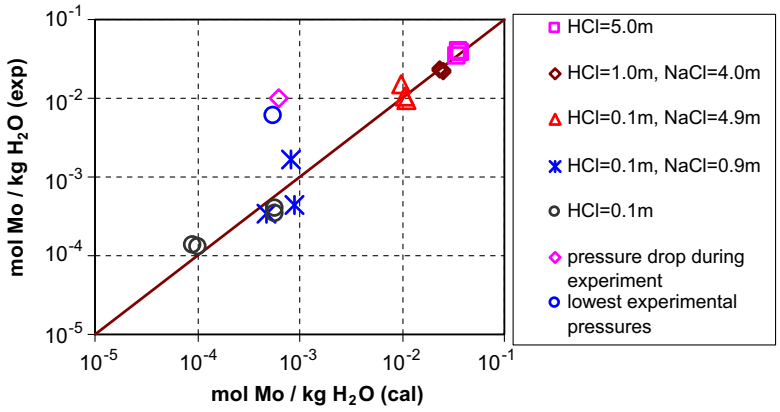

Fig. 3. Parity plot for the calculated and experimental concentrations of Mo(III) in saturated solutions.

(i.e., 5 molal) but different acidity. Specifically, the solubility in a 5 m HCl solution is higher than in a 1 m HCl + 4 m NaCl solution, which is in turn higher than in a 0.1 m HCl + 4.9 m NaCl solution.

The accuracy of reproducing the experimental data by the model is analyzed in Fig. 3, which shows a parity plot of calculated versus experimental concentrations. Most of the experimental data points (i.e., 17 out of 19) are accurately reproduced by the model but two points are in disagreement with the calculated results. These two points do not lie on the diagonal line in Fig. 3 and were both obtained in 0.1 m HCl and 0.9 m NaCl solutions at the lowest partial pressure of hydrogen. One of these two outlying points corresponds to an experiment in which a loss of pressure was observed during the experiment (cf. Table 1) and the other corresponds to the lowest calculated H_2 partial pressure, which is subject to the largest experimental uncertainty, related to the method of calculating the H_2 partial pressure. The speciation of Mo(III) solutions is shown in Fig. 4 for a total concentration of 0.001 m total dissolved Mo(III) at 80 °C and ionic strength of 1.0 m (NaCl). The lines in Fig. 4 have been calculated using the model parameters that are summarized in Tables 2 and 3. In the pH range that is of interest in this study, and also in the range that corresponds to active localized corrosion, Mo(III) is primarily in the form of the unhydrolyzed ion Mo^{3+}. The amount of the hydrolyzed form of Mo(III) (e.g. $MoOH^{2+}$) is less than 10% at pH < 1. The hydrolysis becomes increasingly significant as pH increases and, finally, Mo(III) converts to a neutral species $Mo(OH)_{3aq}$ at pH above ~7. Under the experimental conditions of the solubility studies at the Mo(III)/MoO_2 boundary, the pH values are about 1 or lower. Depending on the total chloride concentration, the primary Mo(III) species may change from Mo^{3+} to the chloride complex, $MoCl^{2+}$. This can be seen from the speciation plots in Figs. 5 and 6, which

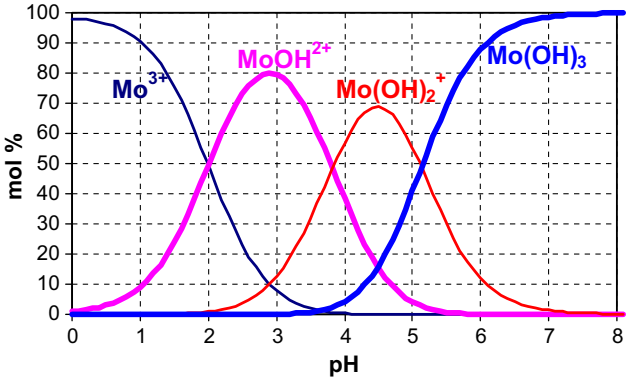

Fig. 4. Predicted speciation of Mo(III) in aqueous 0.001 m solutions (NaCl = 1.0 m) at 80 °C as a function of pH.

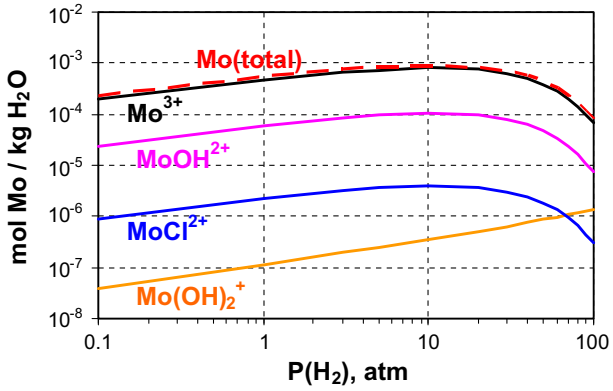

Fig. 5. Calculated concentrations of various Mo(III) species as a function of H_2 partial pressure at the Mo(III)/MoO_2 phase boundary at 80 °C and HCl = 0.1 m and NaCl = 0.9 m. The dashed line indicates the total concentration of dissolved Mo.

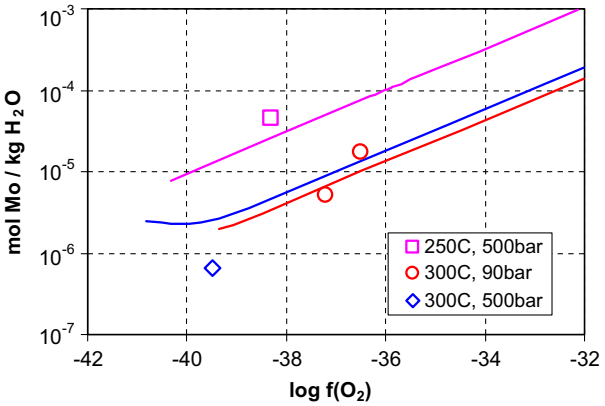

Fig. 7. Calculated and experimental [25] solubility of MoO_2 in water as a function of O_2 fugacity at 250 °C and 500 bar (upper line), 300 °C and 500 bar (middle line), and 300 °C and 90 bar (lower line).

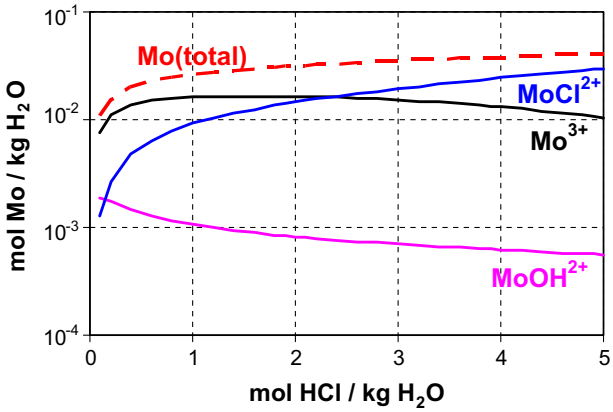

Fig. 6. Speciation of various Mo(III) species as a function of HCl molality at the Mo(III)/MoO_2 phase boundary at 80 °C, P_{H2} = 50 atm, and total chloride concentration (i.e., HCl + NaCl) of 5 molal.

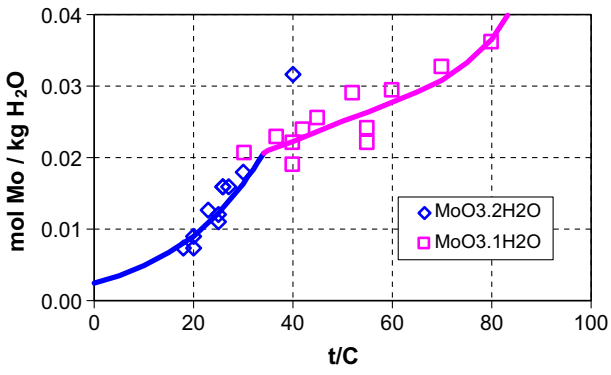

Fig. 8. Calculated and experimental solubility of Mo(VI) in water as a function of temperature. The experimental data are from Linke and Seidell [26], Ferris [27], Cannon [28], Ivanova et al. [29], and Gmelin [30].

are both calculated using the previously determined parameters at the Mo(III)/MoO_2 boundary. In Fig. 5, the saturated solutions contain 0.1 m HCl and 0.9 m NaCl and the primary species is Mo^{3+} with some non-negligible amount (~10%) of the hydrolyzed species $MoOH^{2+}$ over the entire range of H_2 partial pressure studied here. The H_2 partial pressure has a small effect on the relative amounts

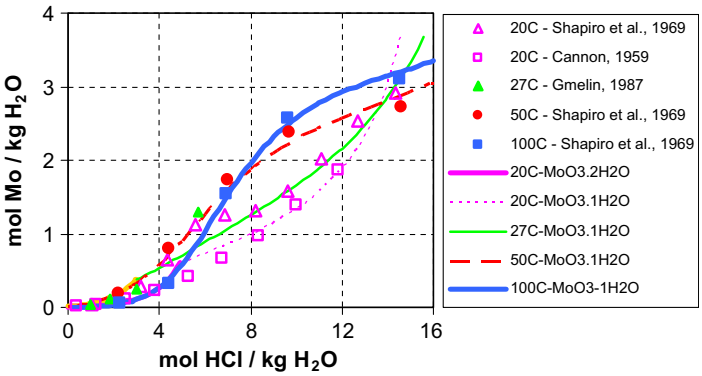

Fig. 9. Calculated and experimental solubility of Mo(VI) in HCl solutions as a function of HCl concentration and temperature. The data are from Gmelin [30], Shapiro and Volk-Karachevskaya [31], and Cannon [28].

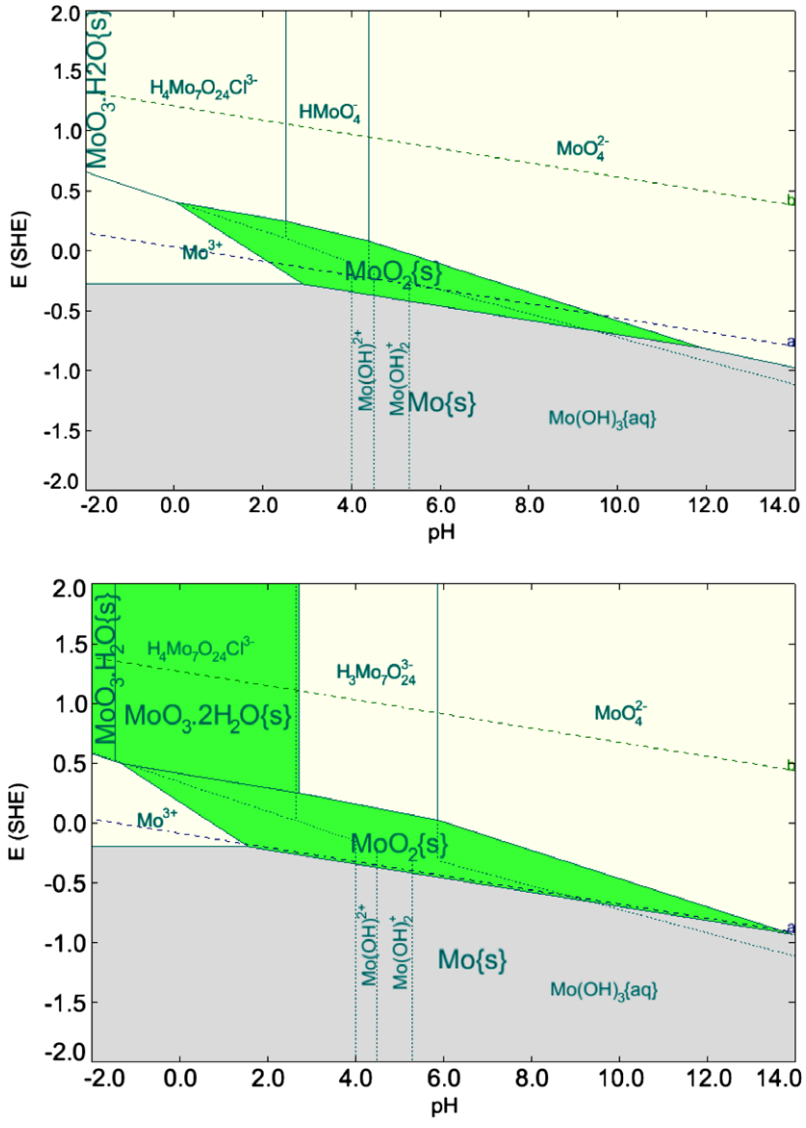

Fig. 10. E-pH diagrams for molybdenum at 25 °C calculated using the new thermodynamic parameters. The upper and lower diagrams have been generated for the activities of dissolved Mo equal to 10^{-6} and 10^{-2}, respectively. The pH has been varied by simulated titration with HCl and NaOH; thus, the concentrations of Cl^- and Na^+ have been varied in lockstep with those of H^+ and OH^-, respectively.

of various Mo(III) species. Fig. 6 has been generated for saturated Mo(III) solutions containing HCl and NaCl with a total chloride concentration of 5.0 molal. The primary species here are Mo^{3+} at lower HCl concentrations and $MoCl^{2+}$, which becomes increasingly significant with rising HCl concentrations. The increase in solubility with H_2 partial pressure and with HCl concentration is consistent with the dissolution reactions:

$$MoO_{2(s)} + 3H^+ + 1/2H_2 = Mo^{3+} + 2H_2O \quad (11)$$

and

$$MoO_{2(s)} + 3H^+ + Cl^- + 1/2H_2 = MoCl^{2+} + 2H_2O \quad (12)$$

In solutions with low ionic strength, the decrease in the solubility with H_2 partial pressure at high P_{H2} is due to the effects of activity coefficients of the primary species (e.g., Mo^{3+} and $MoOH^{2+}$). However, the activities of these species ($a_i = m_i \cdot \gamma_i$) increase with P_{H2} in accordance with the above dissolution reactions.

Figs. 7–9 compare the calculated results with literature data for Mo(IV) and Mo(VI) systems. Fig. 7 shows the solubility of MoO_2 that corresponds to the oxidative dissolution of Mo(IV) with the formation of Mo(VI) ions. Such measurements are subject to considerable uncertainty because they depend on low fugacities of oxygen. Nevertheless, the calculated results are in a satisfactory agreement with the data. Fig. 8 depicts the solubility of Mo(VI) as a function of temperature. Two solid phases – $MoO_3 \cdot H_2O$ and $MoO_3 \cdot 2H_2O$ are stable depending on temperature. In this case, a substantial amount of experimental data is available from various sources. The model calculations agree with the data within experimental scattering. The solubility of the Mo(VI) solid phases in HCl solutions is illustrated in Fig. 9. The observed strong increase in solubility of the $MoO_3 \cdot H_2O$ and $MoO_3 \cdot 2H_2O$ phases as a function of HCl concentration is consistent with the presence of a Cl-containing complex. The experimental data for this system are available from three different sources, [28, 30, 31] which are in a reasonable agreement with each other. The model calculations are in agreement with the data within experimental uncertainty.

It is also of interest to examine the potential – pH (Pourbaix) diagrams that can be generated using the new parameters obtained for Mo species. For this purpose, the algorithm developed by Anderko et al. [33] has been used. The advantage of this algorithm is that it incorporates solution nonideality as quantified by activity coefficients into the generation of E-pH diagrams. Although activity coefficients provide a secondary correction compared with the thermochemical properties of individual species, their inclusion ensures that the diagrams are fully consistent with solubility calculations. Fig. 10 shows the obtained diagrams for the activities of dissolved Mo species equal to 10^{-6} (upper diagram) and 10^{-2} (lower diagram). The diagrams have been generated on the assumption that pH is varied by titrating the solution with HCl and NaOH. Because of the use of HCl as a titrant, the concentration of Cl is varied in lockstep with that of H^+ ions and becomes much larger than the concentration of Mo species in the low pH range. Therefore, chloride complexes of Mo become stabilized in the acidic region. If a different acid was used for the simulated titration, the $H_4Mo_7O_{24}Cl^{3-}$ species would be replaced with a corresponding Mo(VI) species without Cl. The main difference between Fig. 10 and the classical diagrams of Pourbaix [7] lies in the stability fields of $MoO_3 \cdot H_2O$ and $MoO_3 \cdot 2H_2O$ and in the speciation of Mo(III) ions. The stability fields of Mo^{3+} and MoO_2 in the acidic range remain similar. However, the main advantage of the new parameters lies in the accurate representation of the properties of concentrated Mo(III) solutions in the presence of chlorides rather than in improving the properties of dilute solutions, which manifest themselves in E-pH diagrams.

6. Conclusions

To provide a thermodynamic foundation for the study of localized corrosion environments, solubility of Mo(III) species in equilibrium with solid MoO_2 has been determined at 80 °C as a function of solution acidity, chloride concentration and partial pressure of hydrogen. The obtained results have been combined with literature data for systems containing Mo(III), Mo(IV), and Mo(VI) to develop a comprehensive thermodynamic model of aqueous molybdenum chemistry. The model generally reproduces the data within experimental scattering and provides a tool for predicting the phase behavior and speciation in complex aqueous solutions as a function of temperature, acidity, chloride concentration, redox conditions, etc. The experimental and computational results indicate a strong effect of chloride ions on the stabilization of Mo(III) in concentrated solutions. An extension of the model to incorporate other alloy components and to study the chemistry of localized corrosion environments will be the subject of a forthcoming study.

Acknowledgements

The financial support of this work from the Science & Technology Program of the Office of Science and Technology and International (OST&I), Office of Civilian Radioactive Waste Management (OCRWM), US Department of Energy (DOE) is gratefully acknowledged. The experimental work was conducted by LLW, DJW, and JR at Oak Ridge National Laboratory, which is managed and operated by UT Battelle, LLC, under contract DE-AC05-00OR22725 for the US Department of Energy. The interactions among investigators in the OST&I Materials Performance Thrust are appreciated and gratefully acknowledged.

References

[1] R.C. Newman, Corros. Sci. 25 (1985) 331. ibid., 1985, 25, 341.
[2] M. Urquidi-Macdonald, D.D. Macdonald, J. Electrochim. Soc. 136 (1989) 961.
[3] R.S. Lillard, M.P. Jurinski, J.R. Scully, Corrosion 50 (1994) 251.
[4] N.J. Laycock, R.C. Newman, Corros. Sci. 39 (1997) 1771.
[5] J.R. Hayes, J.J. Gray, A.W. Szmodis, C.A. Orme, Corrosion 62 (2006) 491.
[6] F.A. Cotton, G. Wilkinson, Advanced Inorganic Chemistry, A Comprehensive Text, fourth ed., Wiley-Interscience, New York, 1980.
[7] M. Pourbaix, Atlas of Electrochemical Equilibria in Aqueous Solutions, Pergamon Press, New York, NY, 1966.
[8] P. Wang, A. Anderko, R.D. Young, Fluid Phase Equilib. 203 (2002) 141–176.
[9] P. Wang, P. Wang, R.D. Springer, R.D. Young, Fluid Phase Equilib. 222–223 (2004) 11–17.
[10] P. Wang, A. Anderko, R.D. Springer, R.D. Young, J. Mol. Liq. 125 (2006) 37–44.
[11] D.A. Palmer, P. Bénézeth, D.J. Wesolowski, Geochim. Cosmochim. Acta 65 (2001) 2081–2095.
[12] D.G. Archer, J. Phys. Chem. Ref. Data 21 (1992) 793–829.
[13] J.F. Zemaitis, D.M. Clark, M. Rafal, N.C. Scrivner, Handbook of Aqueous Electrolyte Thermodynamics, DIPPR, AIChE, New York, NY, 1986.
[14] K.S. Pitzer, J. Am. Chem. Soc. 102 (1980) 2902–2906.
[15] D.S. Abrams, J.M. Prausnitz, AIChE J. 21 (1975) 116–128.
[16] H.C. Helgeson, D.H. Kirkham, G.C. Flowers, Amer. J. Sci. 274 (1974) 1089–1198. ibid., 1974, 274, 1199–1261; ibid., 1976, 276, 97–240; ibid., 1981, 281, 1241–1516.
[17] J.C. Tanger, H.C. Helgeson, Am. J. Sci. 288 (1988) 19–98.
[18] E.L. Shock, H.C. Helgeson, D.A. Sverjensky, Geochim. Cosmochim. Acta 53 (1989) 2157–2183.
[19] E.L. Shock, H.C. Helgeson, Geochim. Cosmochim. Acta 52 (1988) 2009–2036. ibid., 1990, 54, 915-943.
[20] E.L. Shock, D.C. Sassani, M. Willis, D.A. Sverjensky, Geochim. Cosmochim. Acta 61 (1997) 907–950.
[21] D.A. Sverjensky, E.L. Shock, H.C. Helgeson, Geochim. Cosmochim. Acta 61 (1997) 1359–1412.
[22] M. Rafal, J.W. Berthold, N.C. Scrivner, S.L. Grise, Models for Electrolyte Solutions, in Models for Thermodynamic and Phase Equilibria Calculations, in: S.I. Sandler (Ed.), M. Dekker, New York, NY, 1994, pp. 601–670.
[23] L.I. Mit'kina, N.V. Mel'chakova, V.M. Peshenkova, Russ. J. Inorg. Chem. 23 (1978) 693–695.
[24] T. Kekesi, T.I. Torok, M. Isshiki, Hydrometallurgy 77 (2005) 81–88.
[25] A.V. Kudrin, Geokhimiya 6 (1985) 870–882.

[26] W. F. Linke, A. S. Seidell, Solubilities of Inorganic and Metal Organic Compounds K-Z, vol. 2, fourth ed., American Chemical Society, Washington, DC, 1965.
[27] L.M. Ferris, J. Chem. Eng. Data 6 (1961) 600–603.
[28] P. Cannon, J. Inorg. Nucl. Chem. 11 (1959) 124–127.
[29] G.F. Ivanova, N.I. Lavkina, L.A. Nesterova, A.P. Zhudikova, I.L. Khodakovskiy, Geochem. Int. 12 (1975) 163–176.
[30] L. Gmelin, Gmelin Handbook of Inorganic Chemistry, eight ed., Springer-Verlag, New York, 1987.
[31] K.Ya. Shapiro, I.V. Volk-Karachevskaya, Solubility of molybdic acid in hydrochloric, sulfuric, and nitric acids, Russ. J. Inorg. Chem. 14 (1969) 571–573.
[32] R.M. Smith, A.E. Martell, Critical Stability Constants, Plenum Press, New York, 1989.
[33] A. Anderko, S.J. Sanders, R.D. Young, Corrosion 53 (1997) 43–53.
[34] L.V. Gurvich, I.V. Veyts, C.B. Alcock, V.S. Iorish, Thermodynamic Properties of Individual Substances, vols. 1-5, Hemisphere Publishing Co., New York, 1988-1998.
[35] NIST Chemistry Webbook, NIST Standard Reference Database No. 69, June 2005 Release, National Institute of Standards and Technology, http://webbook.nist.gov/chemistry/.
[36] D.C. Sassani, E.L. Shock, Geochim. Cosmochim. Acta 56 (1992) 3895–3908.
[37] M.S. Gruszkiewicz, D.A. Palmer, R.D. Springer, P. Wang, A. Anderko, J. Sol. Chem. 36 (2007) 723–765.